Tectonophysics 473 (2009) 446–456

Contents lists available at ScienceDirect

Tectonophysics

journal homepage: www.elsevier.com/locate/tecto

The effect of the salt viscosity on future evolution of the Gorleben salt diapir, Germany

Z. Chemia [a,*], H. Schmeling [b], H. Koyi [a]

[a] Hans Ramberg Tectonic Laboratory, Solid Earth Geology, Department of Earth Sciences, Uppsala University, SE-752 36, Uppsala, Sweden
[b] Institute of Earth Sciences, Section Geophysics J. W. Goethe-University Frankfurt Main Altenhferallee 1, 60438 Frankfurt am Main, Germany

ARTICLE INFO

Article history:
Received 21 September 2008
Received in revised form 20 March 2009
Accepted 25 March 2009
Available online 6 April 2009

Keywords:
Salt
Diapir
Anhydrite
Gorleben
Deformation
Rheology

ABSTRACT

The Gorleben diapir, which has been targeted for radioactive waste disposal, contains large blocks of anhydrite. Numerical models that depict the geometrical configuration of the Gorleben diapir are used to understand internal structure of diapir caused by movement of the anhydrite blocks for various salt rheologies. It is shown that the rheology of the salt plays a significant role in how and at which rate the anhydrite blocks sink within the diapir. The mobility of anhydrite blocks depends on the effective viscosity of salt which has to be lower than threshold value of around 10^{18}–10^{19} Pa s. Decreasing salt viscosity allows the previously "stationary" anhydrite blocks to sink. If the effective viscosity of salt in post-depositional stage of the Gorleben diapir falls below this threshold value, induced internal flow due to the present anhydrite layer might disturb any repository within the diapir.

1. Introduction

For the last 40 years, scientist and engineers have been searching for geologically suitable repositions for radioactive waste. Currently only one repository is in use, the Waste Isolation Pilot Plant (WIPP) where long-lived radioactive waste is buried in deep salt beds (40 km east Carlsbad, New Mexico). Salt layers and diapirs have been targeted as waste repository. However, tectonic stability of a salt diapir is a significant factor in evaluating its suitability as a repository for waste disposal. To evaluate safety of a repository many different scenarios have been considered such as: subrosion (dissolving, leaching off) and diapirism, brine migration, thermo-mechanical fractures, flooding of a disposal mine, large brine inclusions, diapirism to the biosphere, solution mining etc. (e.g. Onshore disposal committee, 1989). Many of these scenarios have been applied to Gorleben salt diapir (NW Germany) which is currently used as an intermediate storage facility and was targeted as a future final repository for high-grade radioactive waste. However, the influence of dense inclusions, anhydrite layer, which is present within the Gorleben salt diapir, was not considered as a possible disturbance of the repository. According the current planning the radioactive repository is planned in halite. An approximate level of plant survey is indicated on Fig. 1 (white bar). Based on analogue and numerical models Koyi and Schott (2000) and Koyi (2001) suggested that Gorleben diapir might be active internally due to presence of a dense anhydrite layer (blocks) within it. According to Koyi's (2001) models, the denser blocks, which were entrained by the diapir, sink within the externally inactive Gorleben diapir. Indications for movement of the anhydrite blocks come from acoustic emission measurement that have recorded displacement on the boundary between rock salt and the anhydrite blocks (Spies and Eisenblätter, 2001).

Numerical models carried out by Chemia et al. (2008) showed that sinking of the denser inclusion is inevitable in inactive Newtonian salt diapirs. It has been shown that the growth of salt diapir is relatively insensitive to the rheology of the rising salt itself (Van Keken et al., 1993; Weijermars et al., 1993). However, the rheology of the diapir plays an important role in the entrainment of the embedded dense inclusions (Weinberg, 1993). Therefore, we attribute importance to possible internal activity of the non-Newtonian salt diapirs with intercalated dense layers.

This study models the dynamics of the present configuration within the Gorleben salt diapir. The Gorleben salt is modeled with rheological parameters chosen from laboratory experiments on different salt formations. It is worthwhile to test which rheology is able to activate previously inactive anhydrite blocks.

2. The evolution history of the Gorleben diapir

The Gorleben salt diapir, which roughly trends NE–SW, is about 14 km long and up to 4 km wide. It contains different cycles of the Zechstein salt formation (z2, z3 and z4, Fig. 1). The base of the Zechstein lies at about 3.1 to 3.3 km below the surface. The stratigraphy and the evolution history of the Gorleben diapir are well

* Corresponding author.
E-mail address: zurab.chemia@geo.uu.se (Z. Chemia).

0040-1951/$ – see front matter © 2009 Elsevier B.V. All rights reserved.
doi:10.1016/j.tecto.2009.03.027

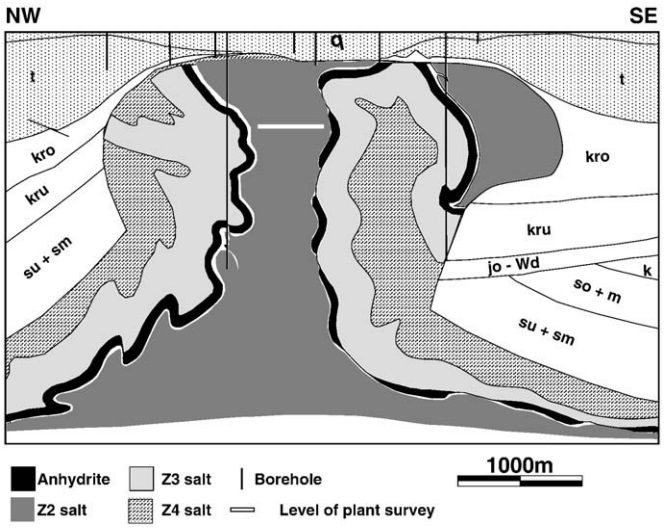

Fig. 1. Line drawing of a northwest–southeast profile of the Gorleben salt diapir in northwest Germany showing entrained segments of dense anhydrite within a diapir. Symbols: q—Quaternary, t—Tertiary, kro—Upper Cretaceous, kru—Lower Cretaceous, so + m—Upper Bunter, su + sm—Buntsandstein. Modified after Bornemann (1991).

explored by four exploratory wells and two shafts that are drilled into the Gorleben diapir, in addition to more than forty wells that explored overlying beds and the salt dissolution zone at the base of the caprock (Bornemann, 1982, 1991).

It is suggested that the salt structures from the Gorleben diapir evolved above an elevation of the basement and the total primary thickness of the Zechstein salt in that area is estimated to be about 1.1 to 1.4 km (Zirngast, 1996). Halokinesis was initiated in the Early Triassic to Middle Triassic, and a thick salt pillow formed during Keuper (Late Triassic) and Jurassic time (Zirngast, 1991; Jaritz, 1993). The diapiric stage was reached in Late Jurassic and Early Cretaceous and the diapir continued into the Tertiary. Maximum rise rates are calculated as 0.08 mm a^{-1} for the Late Cretaceous and less than 0.02 mm a^{-1} in Miocene to recent times (Zirngast, 1996). The internal structure of the Gorleben diapir is very complex, including vertical or steeply inclined and overturned fold axes. A very remarkable feature is the main anhydrite, which forms a key horizon and is folded within the diapir. The main anhydrite is an important layer with respect to nuclear waste storage because of its size and density. It is about 80 m thick and denser (ca. 3000 kg m^{-3}) than the salt (ca. 2200 kg m^{-3}).

3. Modeling strategy

3.1. Governing equations

The gravitationally unstable, multi-layered system, can be described by the equations of conservation of mass, momentum, and composition for a Boussinesq fluid as (e.g., Weinberg and Schmeling, 1992).

$$\nabla \cdot u = 0 \tag{1}$$

$$0 = -\nabla P + \frac{\partial \tau_{ji}}{\partial x_j} - \rho g \tag{2}$$

$$0 = \frac{\partial c_k}{\partial t} + u \nabla c_k \tag{3}$$

where inertial forces are neglected, and u, P and τ_{ji} are the flow velocity, pressure, and deviatoric stress tensor, respectively. ρ is density, g—gravitational acceleration, t—time, and c_k—concentration of the k-th chemical component. The viscous stress is related to the velocity field by the constitutive equation

$$\tau_{ij} = \eta\left(\frac{\partial u_i}{\partial x_j} + \frac{\partial u_j}{\partial x_i}\right) \tag{4}$$

where η is the viscosity. The Eqs. (1) and (2) are solved using a two-dimensional finite differences (FD) code (FDCON modified after H. Schmeling). The system of the FD equations is solved using a stream function formulation for the momentum equation and by applying Cholesky decomposition of the symmetric matrix. For the conservation of composition (Eq. (3)), a marker approach is used. The markers technique is very effective for multi-compositional flows where each composition has a different rheological property and density. Different chemical compositions (i.e. layers) may be assigned different densities and rheologies. A full description of the mathematical formulation and its numerical implementation are given in Weinberg and Schmeling (1992).

The problem of the numerical diffusion due to moving compositional field (Eq. (3)), which contain sharp discontinuities and might lead to mixing at boundaries between different materials is overcome by defining an effective viscosity for these regions. In mixtures of different compositions, an effective viscosity may be defined by assuming that the total strain rate is given as the weighted sum of the strain rates in each component, or assuming that the total stress is given as the weighted sum of the stresses in each component. Accordingly, the effective viscosity would be given as the harmonic or the arithmetic mean of the viscosities of the components, respectively. As it is not possible to specify which of these means is to be preferred in a complex flow field (see Schmeling et al., 2008, for a comparison of different averaging schemes), the effective viscosity of a mixture is defined here as the geometric mean as:

$$\log \eta = \sum_k c_k \log \eta_k \tag{5}$$

Although a discontinuous rheological boundary is associated with a discontinuous strain rate, the finite difference algorithm used here properly resolves the flow around high viscosity bodies such as the anhydrite blocks in our models. Schmeling et al. (2008) carried out a resolution test for 2D Stokes flow around a high viscosity body using the geometric mean for grid points near the boundary (Eq. (5)). From these results we estimate that the flow around the anhydrite bodies (containing at least 5 grid points) may be erroneous by up to 5%.

3.2. Estimation of rheological behavior

The mechanical properties and their role in the deformation are governing the flow of the materials that form diapiric structures. Basic rheological equations, constitutive equations, which relate stress and strain, are usually derived empirically in laboratory conditions. Many studies have focused on experimental deformations of the steady state flow properties and processes of natural rocksalt. The sets of the steady-state data fit well power law creep relation.

$$\dot{\varepsilon} = A^* \cdot \sigma^n \cdot \exp\left(\frac{-H}{RT}\right) \tag{6}$$

where $\dot{\varepsilon}$ is the steady-strain creep rate, $\sigma = (\sigma_1 - \sigma_3)$ is the stress difference of the maximum and minimum principal stresses, T is absolute temperature, A^* is a material constant, n power law exponent, and $H^* = E^* + PV$ is the activation enthalpy. E^* is the activation energy, V is the activation volume, and P is the (lithostatic) pressure.

Numerical models presented in this study are based on an approach where power-law ductile creep describes deformation

Table 1
Model parameters: A^* is a pre-exponential constant, H^*—activation enthalpy, n—power-law exponent, T_t–T_b is temperature at top and bottom, respectively.

Model	Natural Rocksalt	A^* [Pa^{-n} s^{-1}]	n	H^* [kJ mol^{-1}]	T_t–T_b [°C]	Effective viscosity of salt [Pa s]			Comments
						η_{min}	η_{max}	$\bar{\eta}$	
PF	Paradox Formation	6.9183×10^{-16}	1.39	28.80	0–140	2.29×10^{16}	2.29×10^{18}	2.6×10^{18}	
PF-Cold	Paradox Formation	6.9183×10^{-16}	1.39	28.80	0	8.6×10^{17}	1.9×10^{19}	1.09×10^{19}	
PF-NA	Paradox Formation	6.9183×10^{-16}	1.39	28.80	0–140	7.14×10^{16}	3.2×10^{19}	9.7×10^{18}	No anhydrite
AI	Avery Island	1.4454×10^{-32}	4.10	33.6	0–140	5.9×10^{18}	1.7×10^{23}	1.29×10^{20}	
AI-OV21	Avery Island	1.4454×10^{-32}	4.10	33.6	0–140	$1.7E\times10^{18}$	2.7×10^{22}	5.2×10^{19}	Overburden viscosity is 10^{21} Pa s
AI-OV22	Avery Island	1.4454×10^{-32}	4.10	33.6	0–140	6.2×10^{18}	1.7×10^{22}	8.9×10^{19}	Overburden viscosity is 10^{22} Pa s
VD	Vacherie Dome	4.1687×10^{-16}	2.22	62.90	0–140	5.7×10^{16}	1.0×10^{21}	1.05×10^{19}	
RD	Richton Dome	2.2387×10^{-32}	5.01	82.30	0–140	2.9×10^{19}	1.0×10^{25}	4.3×10^{20}	
SF	Salado Formation	1.5488×10^{-35}	4.90	50.20	0–140	4.0×10^{19}	1.0×10^{25}	4.2×10^{20}	
PB	Permian Basin	4.6774×10^{-30}	4.50	72.00	0–140	2.9×10^{19}	9.8×10^{24}	4.0×10^{20}	
N17	Newtonian	10^{17}	1	–	0–140	–	–	–	
N18	Newtonian	10^{18}	1	–	0–140	–	–	–	

η_{min}, η_{max} and $\bar{\eta}$ are minimum, maximum and arithmetic mean of the salt viscosity occurring in models, respectively.

behavior of the rock. The viscosity depends non-linearly on deviatoric stress, which is given as:

$$\eta = A \cdot \exp\left(\frac{H^*}{RT}\right) \cdot \tau_{II}^{1-n} \tag{7}$$

where $A = \left(3^{\frac{n+1}{2}} \cdot A^*\right)^{-1}$ is a pre-exponential constant, and τ_{II} is the 2nd invariant of the deviatoric stress tensor. Assuming in Eq. (7) that $H^* = 0$ and T= constant, temperature independent power-law ductile creep is given as:

$$\eta = A \cdot \tau_{II}^{1-n} \tag{8}$$

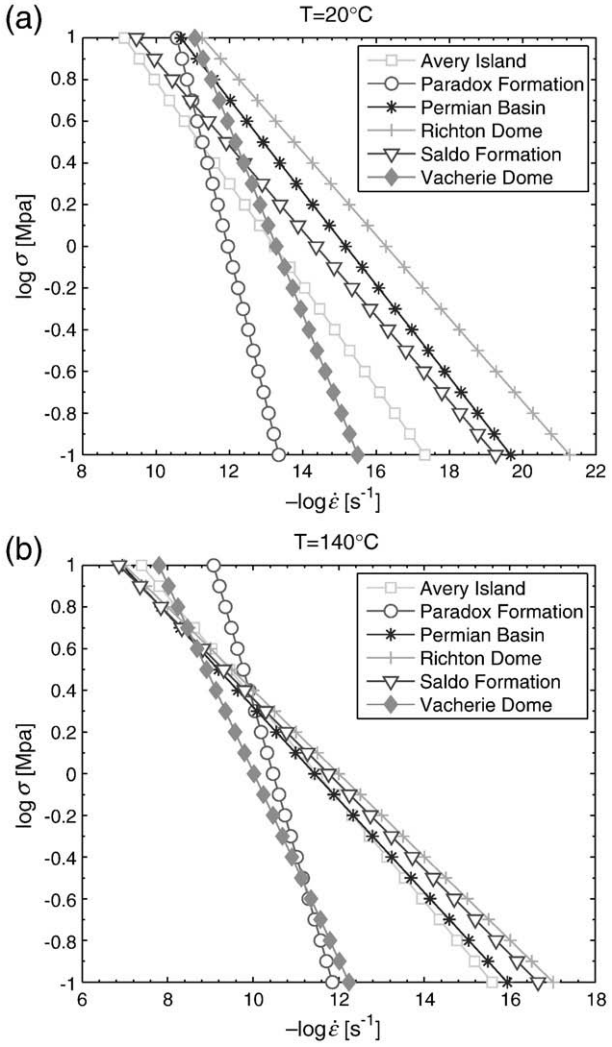

Fig. 2. Deformation map for rocksalt of different formations constructed using the creep law (Eq. (6)). Stress is varied from 0.1 MPa to 10 MPa. a) Temperature is 20 °C. b) Temperature is 140 °C.

Different rheology of the natural rocksalt (e.g. Paradox Formation, Avery Island, Permian Basin, Salado Formation, Richton Dome, and Vacherie Dome; Table 1.) is used to model internal dynamics of the Gorleben salt diapir. Comparison of different creep laws, where stress is varied from 0.1 to 10 MPa and temperature from 20 °C to 140 °C shows that the rocksalt from the Paradox Formation is less stress sensitive than the other salt formations and it shows high strain rate at relatively small stresses (Kirby and Kronenberg, 1987, Fig. 2).

Although salt compositions vary from one formation to another, the rheological behavior is qualitatively similar. The domal salt at Gorleben, for example, has significantly lower water content (ca 0.1–0.2%) and creeps more slowly (Fairhurst, 2002). The microstructures studied in Zechstein samples from Germany and Poland (Asse, Gorleben and Klodawa salt diapirs) shows clear evidence for dislocation creep (Schléder, 2006). Yet, flow laws essentially similar to those in Fig. 2 can be used to study internal dynamics of the Gorleben diapir.

Deformation experiments on anhydrite rocks showed that the strength of the fine-grained anhydrite is strongly temperature and strain-rate dependent above 300 °C whereas coarse grained anhydrite

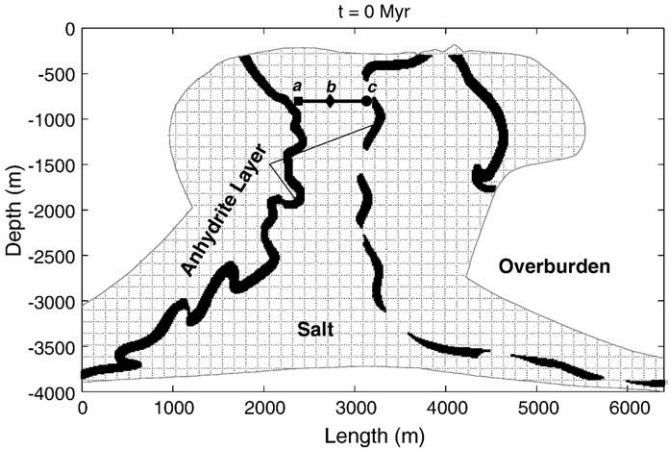

Fig. 3. The initial geometry of the model. The box has no-slip at the bottom, free-slip at the top and reflective side boundaries. The box can be considered as showing the right hand half of a symmetric structure. The temperature distribution within the box linearly varies with depth at the surface 0 °C and 140 °C at the bottom. Points *a*, *b* and *c* define passive markers used to monitor deformation of the plant survey.

rock remains relatively insensitive to strain-rate and temperature even at 450 °C. Although anhydrite has a high strength at room temperatures, fine grained aggregates weaken rapidly above temperatures of 100 °C to 200 °C depending on grain size and strain rate (Muller et al., 1981).

Even though an anhydrite can undergo phase transition to gypsum there is no evidence of such transition within the Gorleben diapir. The reason is that anhydrite is embedded within the salt and does not have a contact with water. The absence of water in the system is another argument for planning the repository within the Gorleben diapir. Therefore, taking into account that the temperature variation in our models is 0–140 °C and that the fine grained anhydrite weaken rapidly above temperatures of 100 °C to 200 °C (Muller et al., 1981) we assume that the anhydrite layer does not undergo significant change in rheology.

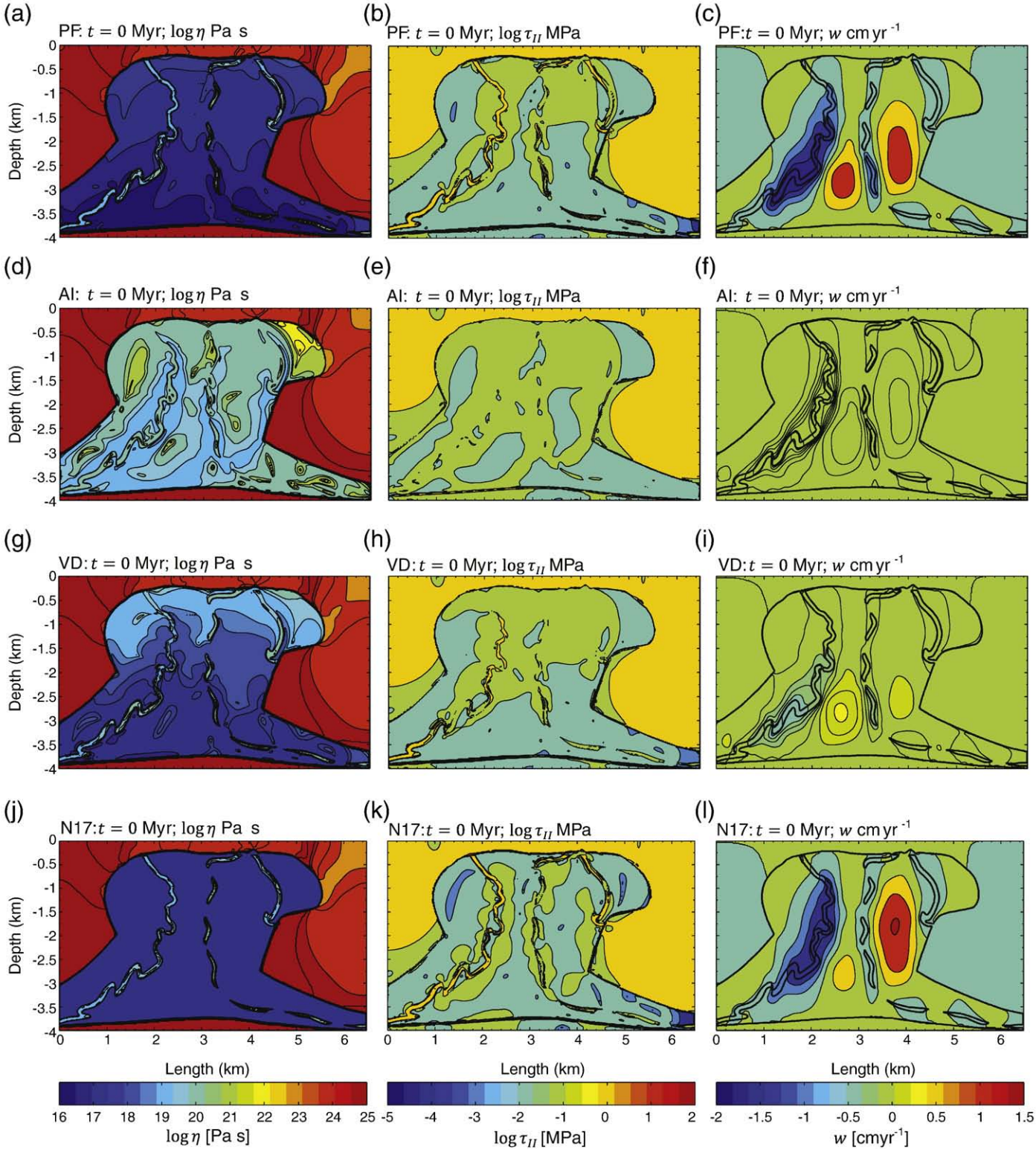

Fig. 4. Initial viscosity, shear stress and vertical velocities for models with different salt rheology. (a–c) Paradox Formation (PF), (d–f) Avery Island (AI), (g–i) Vacherie Dome (VD), (j–l) Newtonian salt with viscosity 10^{17} Pa s. In model AI maximum vertical velocity does not exceed 0.003 cm a^{-1}.

We model anhydrite as a competent layer embedded within the salt layer with a power-law rheology independent of temperature and a low value for the exponent, $n=2$, $A^*=3.08\times10^{-27}$ Pa^{-n} s^{-1} (Muller et al., 1981).

4. Model setup

In this study, we use currently available interpretation of the internal structure of the Gorleben diapir as the initial configuration of the models (Fig. 1). The complex internal stratigraphy of the Gorleben diapir is simplified so that only the Main Anhydrite layer is used in the modeling (Fig. 3). The Main Anhydrite layer is modeled as an average 80 m thick, dense layer (2900 kg m^{-3}) embedded within the Zechstein salt formation. In all models an effective viscosity of anhydrite is between 10^{19} and 10^{21} Pa s.

The sedimentary overburden rocks simulated in all the models are assumed to be static and given corresponding depth-independent density (2600 kg m^{-3}). This assumption is based on the interpretation that the stratigraphic markers in the sediments visible in Fig. 1 have been recorded only during the early active stage of the diapir (downbuilding). It is also known that the diapir has been inactive for last 20 Myr (Zirngast, 1996) which is the reason why the Gorleben

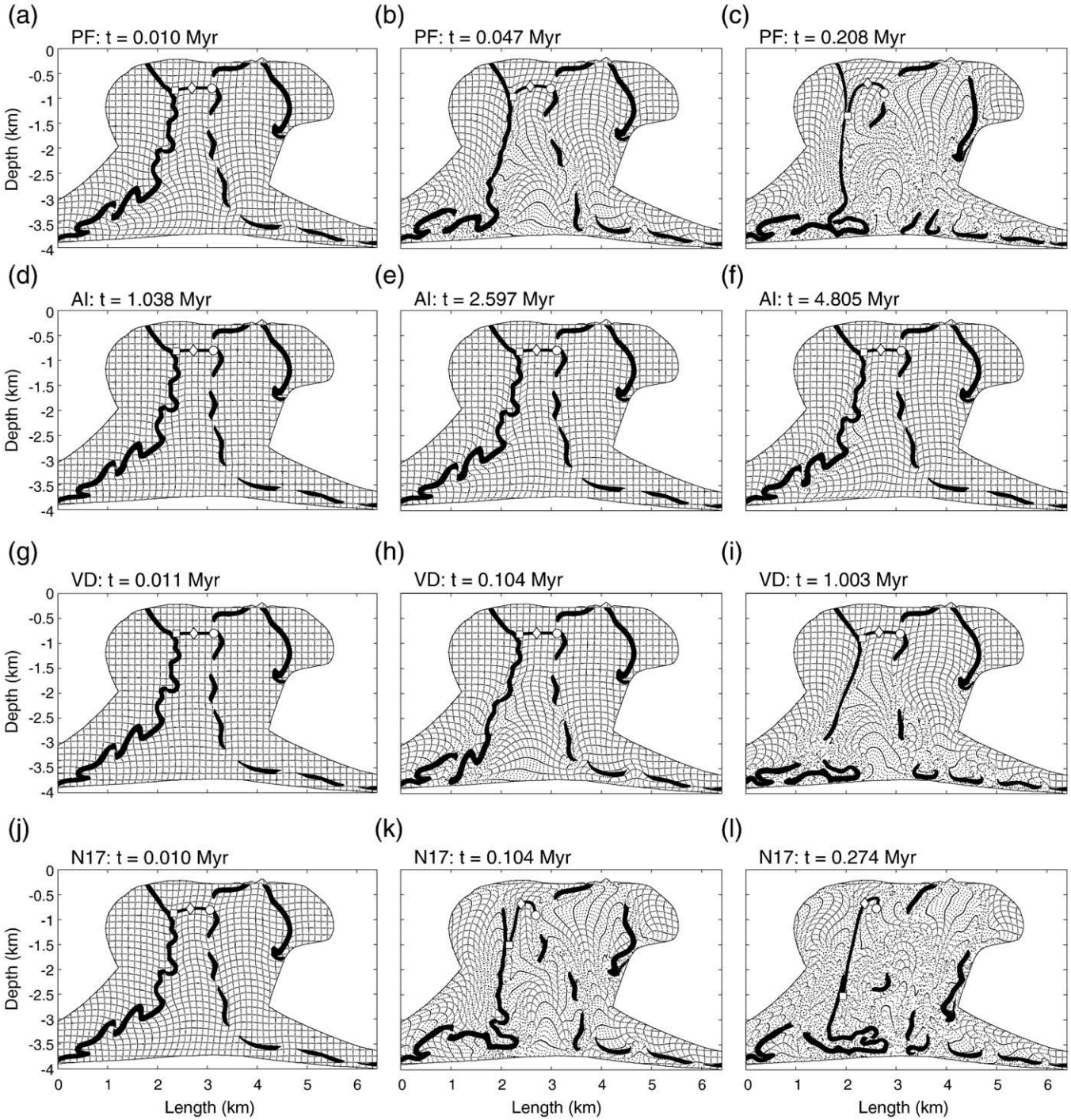

Fig. 5. Evolution of the models for different salt rheology. (a–c) Paradox Formation (PF), (d–f) Avery Island (AI), (g–i) Vacherie Dome (VD), (j–l) Newtonian salt with viscosity 10^{17} Pa s.

diapir has been targeted for radioactive waste disposal. In addition, most sedimentary rocks (clastic or carbonate) behave as non-Newtonian material or as brittle solids, rather than ductile fluids, depending on factors such as their depth of burial, etc. (Vendeville and Jackson, 1992). Thus, a high viscosity (effective viscosity ranges between 10^{23} and 10^{25} Pa s) is assigned to the overburden. This assumption of a very high viscosity keeps ductile deformation in the overburden extremely small. Viscosity contrast between 10^2 and 10^4 for the salt and overburden layers is reported to be a good approximation (Rönnlund, 1989; Hughes and Davison, 1993).

The different cycles of the Zechstein salt z2, z3 and z4 represent the salt layer above the basement (Figs. 1 and 3). The Zechstein salt formation is modeled as a power law salt using rheological parameters chosen from laboratory experiments on different salt formations (Table 1., Kirby and Kronenberg, 1987). These experimental results demonstrate that the variety of salt formations show different rheological behaviors (Fig. 2). A mean value of the density for rock salt is assumed to be 2200 kg m^{-3} (Landolt-Boernstein, 1982). For comparison, Newtonian salt has been modeled with an average viscosity ranging between 10^{17} and 10^{18} Pa s (Urai et al., 1986; Spiers et al., 1990; Carter et al., 1993; Van Keken et al., 1993).

We model in a 4×6.4 km box, which has a no-slip bottom boundary, a free-slip top boundary, and reflective lateral boundaries. The temperature distribution within the box linearly varies with depth (at the surface 0 °C and 140 °C at the bottom). All calculations use 401×251 grid resolution and 2014×1248 markers. The influence of the grid resolution on velocity field is checked in few runs where only this parameter was varied. The results show that the lower resolution models slightly underestimate the velocities. A coarse finite difference grid of only 257×161 nodes and 800×1291 markers reproduce similar solution for the flow fields and velocities at $t=0$ differ by 0.12%.

Our numerical models do not include the effects of neither salt loss by dissolution nor sediment compaction. After initiation, each model is run up to five million years and relative displacement of the potential repository is monitored using the passive markers that are defined at approximately 800 m depth (Fig. 3; points *a*, *b* and *c*). In all model runs, densities and rheologies of the overburden and anhydrite layers are constant whereas, viscosity of the salt is varied (Table 1).

5. Results

In all models, the density contrast between the anhydrite layer and the salt is sufficient to initiate a downward motion of the anhydrite blocks within the diapir (Fig. 4). However, the rate of descent of anhydrite blocks depends on effective viscosity of salt.

In models where the effective viscosity of salt is low (e.g., models for the rocksalt from the Paradox Formation (PF) with effective viscosity of salt between 2.3×10^{16} and 2.3×10^{18} Pa s, and Vacherie Dome (VD) with effective viscosity of salt between 5.7×10^{16} and 10^{21} Pa s; Fig. 4), viscous drag cannot maintain anhydrite blocks at initial levels. The anhydrite blocks sink in these models (Fig. 5a–c and g–i). Due to the complex asymmetric geometry of anhydrite and depth-dependence of the salt rheology, the sinking rate of the anhydrite blocks varies with space and time (Figs. 4 and 5). Larger blocks (western side of the model) begin to sink at a higher rate than in the eastern side of the model where the anhydrite layer is segmented into separate blocks of smaller size (Fig. 5). An average descent velocity of the disrupted anhydrite blocks (eastern side) does not exceed 0.9 mm a^{-1}, whereas the large anhydrite blocks (western side) sink with a velocity of ca. 1 cm a^{-1} at early stages (Fig. 6). Interestingly, even though the western anhydrite body is competent and mechanically connected to the supporting top and bottom of the salt dome, it sinks faster than the eastern mechanically free blocks. As can be seen from Fig. 5, this is due to effective unfolding of the western anhydrite layer accommodated by thinning at later stages.

It is interesting to note, that different activation enthalpies may lead to significantly different behavior: A smaller activation enthalpy of the PF-model (28.8 kJ $mole^{-1}$) results in weak depth dependence of the salt viscosity (Fig. 4a) in contrast to a larger activation enthalpy (62.9 kJ $mole^{-1}$) of the VD-model (Fig. 4g). Accordingly, deformation and anhydrite sinking takes place within the entire dome or only in the lower part, respectively (Fig. 5c, i).

In contrast, salt that is more viscous (e.g., models for the rocksalt from the Avery Island (AI), Richton Dome (RD), and Salado Formation (SF), with effective viscosity of salt greater than 10^{19} Pa s) retards the rate of descent of anhydrite blocks (Fig. 5d–f). Model using the rheology of Avery Island salt, which has been used intensively in steady-state flow experiments because of its purity (>99% halite), homogeneity and relatively small (7.5 mm) average crystal size, results in variation of effective viscosity greater than 10^{20} Pa s and as much as 10^{23} Pa s. In this model, the initiated maximum descent rate of the anhydrite blocks does not exceed 0.03 mm a^{-1}.

In all models, with power law salt rheology, deformation is localized in the vicinity of anhydrite blocks, also reducing the effective

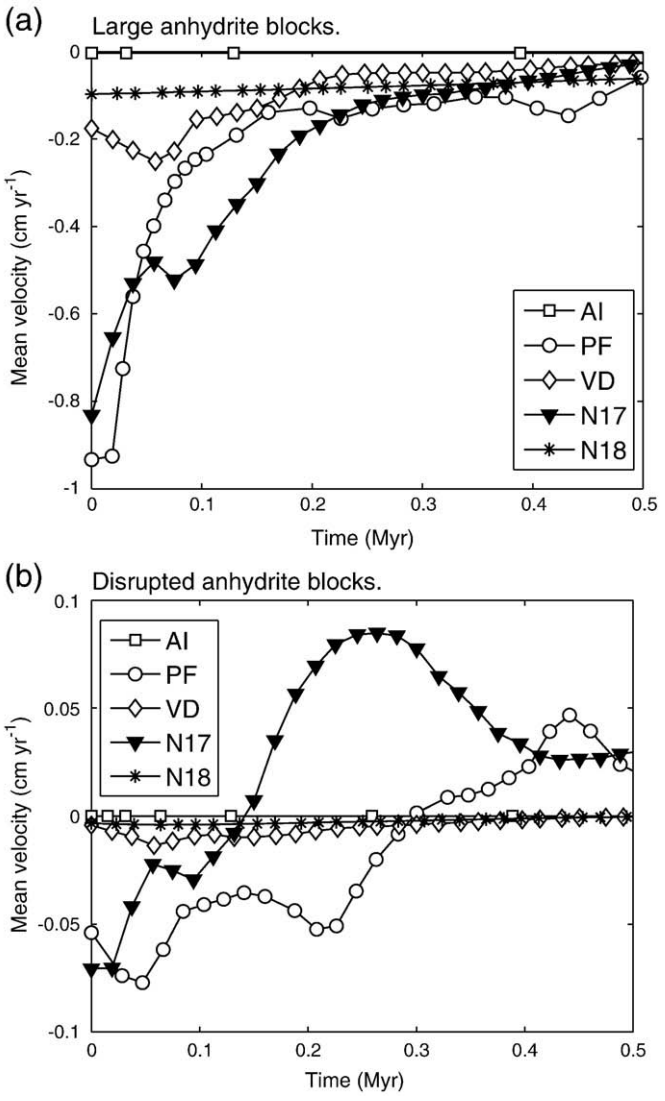

Fig. 6. An average anhydrite velocity versus time for models with different salt rheology. a) West side of the diapir, large anhydrite blocks. b) East side of the diapir, disrupted anhydrite blocks. Symbols: PF—Paradox Formation, VD—Vacherie Dome, AI—Avery Island, N17—Newtonian salt with viscosity 10^{17} Pa s, and N18—Newtonian salt with viscosity 10^{18} Pa s. Models with salt rheology RD—Richton Dome, SF—Salado Formation, PB—Permian basin are similar to AI—Avery Island.

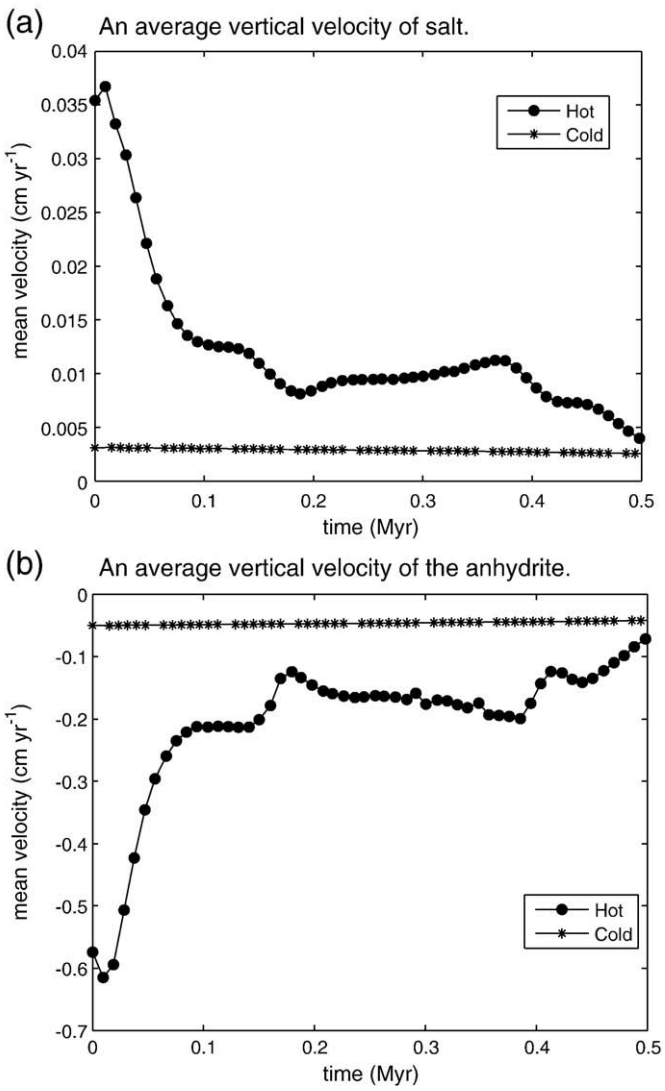

Fig. 7. The effect of temperature on model PF (Paradox Formation salt rheology). a) An average vertical velocity of salt versus time. b) An average vertical velocity of the anhydrite versus time. Hot: temperature distribution within the model linearly varies with depth at the surface 0 °C and 140 °C at the bottom. Cold: temperature is 0 °C within the model.

viscosity of the salt in these regions. Therefore, it is worthwhile to test how the Newtonian rheology of salt affects the internal dynamics of the diapir during the sinking of the anhydrite blocks. In the model where only the diapiric body of salt is modeled with Newtonian rheology (10^{17} Pa s), after initiation, salt flow is initiated by sinking of the embedded anhydrite blocks. The negative buoyancy causes relative displacement within the diapir. The vertical salt flow (5 mm a^{-1}) is initiated in the middle of the model, which results in uplift of the structures between the anhydrite layers. As the Newtonian salt rheology does not have temperature dependence, the salt viscosity is no more depth dependent. The sinking blocks within the Newtonian salt diapir deform larger volume of the salt (Fig. 5). However, by increasing the viscosity of salt by a factor 10 to 10^{18} Pa s, the internal flow and, thus, the internal deformation of the diapir are reduced by approximately the same factor.

6. Discussion

The results of the numerical models show that a diapir remains stable (inactive) for millions of years if the diapir is covered with stiff overburden layers (i.e. effective viscosity ranges between 10^{23} and 10^{25} Pa s). However, if the diapir includes dense blocks, depending on effective viscosity of the salt, such a diapir may deform internally.

In order to assess the potential importance of sinking or mobility of entrained blocks within a diapir, it is important to understand how an anhydrite layer was entrained into a diapir. The following time-scales has to be considered: the time scale of diapiric growth t_1 (e.g. by down-building) and the time scale of sinking of the blocks, t_2. Keeping all material parameters the same, entrainment of dense blocks require that $t_1 < t_2$, i.e. during diapiric rise the rheology of the salt has to be sufficiently stiff to entrain the dense anhydrite blocks, the blocks do not sink faster than the diapir grows (Weinberg, 1993; Chemia et al., 2008).

As the time scale of sinking of the blocks, t_2 controls the mobility of the blocks, the condition $t_2 > t_1$ has implicitly been taken as a guarantee for the safety of the stability of the waste repository. The growth rate of the Gorleben diapir is approximated to be 0.02 mm a^{-1} from Miocene (Zirngast, 1996). The anhydrite blocks remained in place for the last 20 Myr, or if they were sinking, the deformation rate was so slow that most of the anhydrite layer is still present at shallow depth. Our numerical models with Newtonian salt and power-law salt of the Vacherie Dome and Paradox Formation show that the dense anhydrite

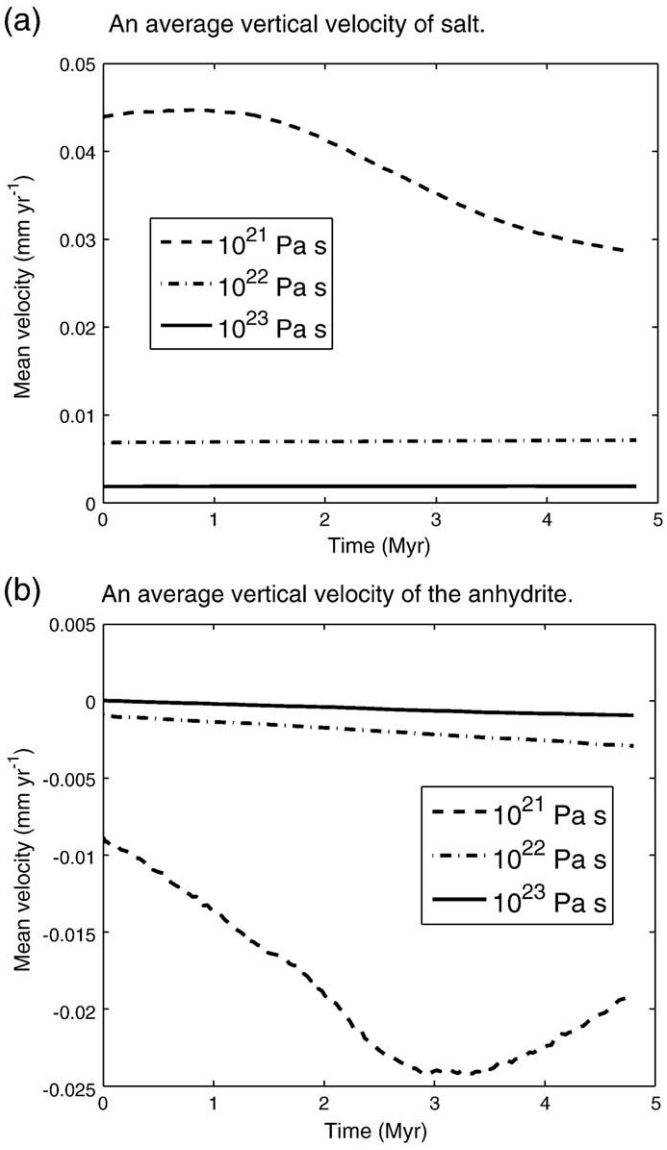

Fig. 8. The effect of overburden viscosity on model AI (Avery Island salt rheology). a) An average vertical velocity of salt versus time. b) An average vertical velocity of the anhydrite versus time. Overburden viscosity is varied form 10^{21} Pa s to 10^{23} Pa s.

blocks sink fast and reach the bottom in less than one million years. This observation suggests that if the average effective viscosity of salt ranges from 10^{17} to 10^{18} Pa s (e.g., Urai et al., 1986; Spiers et al., 1990; Hunsche and Hampel, 1999) diapirs with intercalated denser layer must be internally active even though the surface of the diapir does not rise Koyi (2000, 2001), Chemia et al. (2008), Chemia and Koyi (2008). The fact

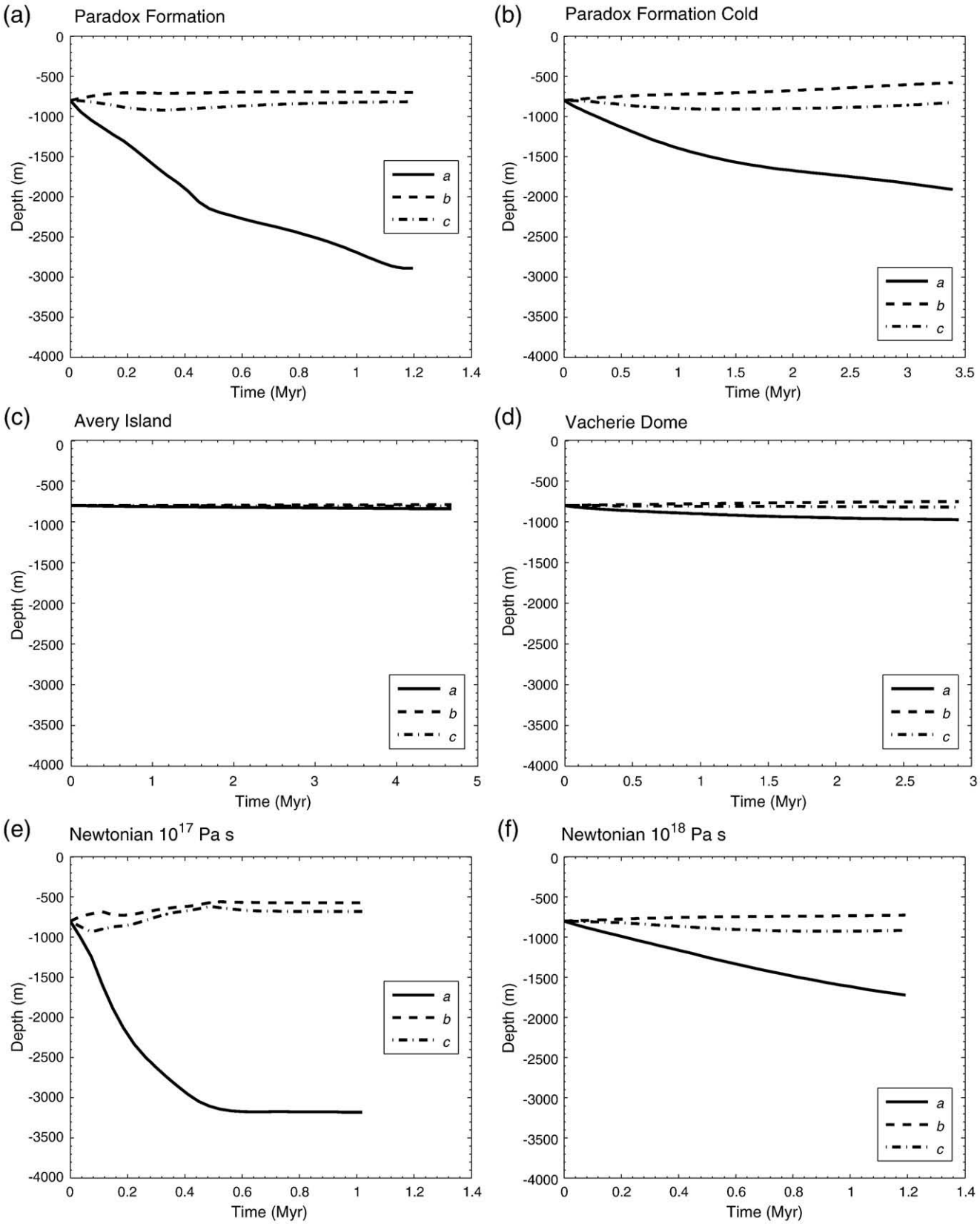

Fig. 9. The vertical displacement for passive markers in different models. Models RD—Richton Dome, SF—Salado Formation, PB—Permian basin are similar to AI—Avery Island.

that the internal movement of the diapir is due to the presence of the anhydrite layer is verified in the model where the anhydrite layer was removed from the initial setup, but all the other parameters were kept the same. In this model salt remained inactive (maximum vertical velocity 9.6×10^{-5} mm a^{-1}) both externally and internally for more than 5 million years.

An acoustic emission measurement confirm displacement on the boundary between rock salt and the anhydrite blocks (Spies and Eisenblätter, 2001). The emissions can be triggered by density contrast between the rigid anhydrite and the ductile salt or by excavating cavities near anhydrite. The redistribution of stresses around the cavity lead to deviatoric stresses at the boundary between ductile salt and the anhydrite, which has higher strength than salt and is brittle (Spies and Eisenblätter, 2001). In either case, the ductile rheology of salt accommodates the brittle deformation, and therefore salt rheology controls the sinking rate of the anhydrite and the style of deformation.

The curvature of the anhydrite layer (Fig. 11a) illustrates that the blocks have been sinking. If the anhydrite blocks have been active recently, the second time scale t_2 seems to have dropped considerably, which can only be the case if the rheology of the salt has changed after emplacement.

An increased mobilization of the intercalated heavy blocks require processes with a time scale between 0 and 10 Myr weakening the rheology during this late stage. Possible processes include: (a) Migration or diffusion of water through the salt phase during the late stage. A possible cause could by a change in sub-glacial groundwater pressure induced by past or future glaciations (Talbot, 1999). (b) Heating by time-dependent hydrothermal convection in the surrounding sediments, driven by close geothermal anomalies or exogenic forces, (time scale down to years). (c) Localized heating by future radioactive waste disposal. Any of these processes, which might already have taken place, can change the rheology of salt.

A thorough assessment of these or other processes lies beyond the scope of this paper. However, inspection of the temperature dependence of the salt rheologies summarized in Table 1 shows that a temperature increase from 20 to 140 °C is accompanied by about 2 to 4 orders of magnitude decrease in effective viscosity of salt. Therefore, the descent velocity of the anhydrite would increase compared to the "colder" state. This effect is tested in an end member model in which the temperature is cold everywhere in the diapir. In this case, the salt velocity and the sinking velocity of the anhydrite are much smaller than in the case for a linear temperature increase with depth (Fig. 7).

The rate of salt flow within a diapir and thus the rate of decent of the anhydrite blocks can be altered by variation in regional stresses, as the effective viscosity of a non-Newtonian rheology depends also on the background stress. However, this mechanism is unlikely to account for mobilization of anhydrite blocks because of the following reason: In order to generate a hypothetical post-emplacement reduction of the salt viscosity by a change in regional stress, the strain rates in the salt due to the mobilized anhydrite blocks and due to the enhanced regional stress within the salt have to be of the same order. Thus, the shape of the salt dome has to change with the same rate as the blocks sink. Furthermore, due to the competence contrast between salt and surrounding rock, a change in regional stress of the surrounding rock does not lead to a notable change of the state of stress within the salt.

One of the parameters controlling stresses in the overburden is the viscosity contrast between the whole overburden and the salt. However, the sharp viscosity contrast between the salt and the overburden (>5 orders of magnitude) leads to spurious stress concentrations along the salt–sediment-interface, which show up if, one zooms in at the interface in Fig. 4. These can be disregarded as the stress is calculated a posteriori, and the flow solution uses the rheology formulation based on the strain-rate-dependence. Thus, the spurious stress concentrations do not affect the flow solution.

We use high viscosity overburden to simulate postdiapirc state of the Gorleben diapir. In analogue models often the postdiapiric state is simulated by a critical thickness of the overburden (Biot, 1965; Koyi and Mancktelow, 2001). Alternatively, sufficiently stiff overburden can be used to simulate inactive diapirs (Biot, 1965). Since the thickness of the overburden for Gorleben diapir is well known and it is reported that the diapir is externally inactive we used stiff overburden approach. However, the results of the numerical models, with lower viscosity contrast between the overburden and the salt elucidate the importance of the overburden layers, which causes viscous drag along their boundaries with the salt. The results show that by decrease in overburden viscosity, the wall of the salt is no more rigid and the velocity in the salt is faster (Fig. 8). The overburden deforms and drives the salt upwards. If the contrast between the Newtonian overburden and non-Newtonian salt viscosities is less than 10^2, the effective viscosity of salt is reduced. This results in high mobility of the anhydrite blocks (Fig. 8). Furthermore, if the overburden viscosity is similar to salt the anhydrite layer sinks fast at initial stages but later on it is entrained by upward flowing salt. Models in which the overburden viscosity is reduced, illustrate that low viscosity overburden aids the mobility of anhydrite blocks through altering the effective viscosity of salt.

6.1. Deformation of the repository

Based on the movement of passive markers, it is suggested that for the salt modeled with (weakest) rheological parameters of the Paradox Formation, the western margin of the potential repository (adjacent to larger anhydrite blocks, point a) will sink with an average rate of 3.2 mm a^{-1} during a subsequent time period of 0.1 Ma. The

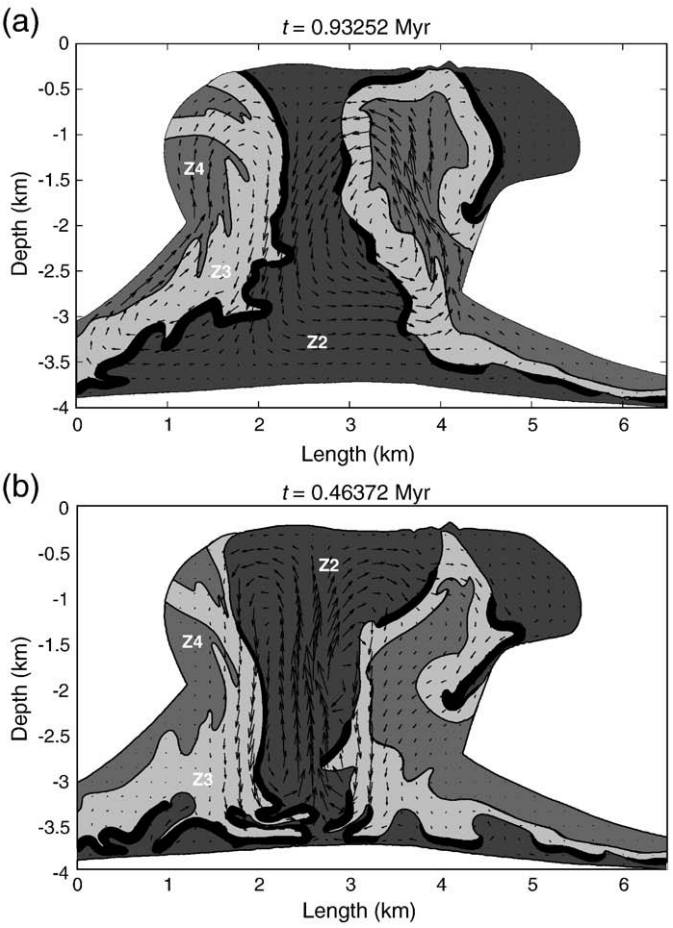

Fig. 10. Snapshots of two multilayered salt models with arbitrary chosen Newtonian salt rheologies. a) The viscosity of z2 layer is 10^{19} Pa s, z3 is 10^{18} Pa s and z4 is 10^{17} Pa s. b) The viscosity of z2 layer is 10^{17} Pa s, z3 is 10^{18} Pa s and z4 is 10^{19} Pa s.

eastern margin of the potential repository (point *c*) will sink with a rate of 0.2 mm a^{-1} within the same time. Unlike marginal points of the potential repository, the mid-point (point *b*) rises with a rate of 0.73 mm a^{-1}. The deformation rate of the potential repository is sufficiently reduced if the effective viscosity of salt is high (models: AI, SD, RD, and PB, Fig. 9). This observation suggests that if the average effective viscosity of salt ranges from 10^{19} to 10^{20} Pa s the diapirs with intercalated denser layer must deform with a rate that is not significant (often the diapirs with rate of rise of surface less than 0.02 mm a^{-1} are considered as inactive). It should be noted that the fast deformations rates predicted if the weak PD-rheology is assumed lie in the range to be observed by geodetic measurements. The fastest descent rate is observed in models with an average viscosity of salt 10^{17} Pa s.

6.2. Rheology of different salt layers

In salt diapirs small and large scale folding is very likely caused by the differences in mechanical properties in the salt layers (Ramsay, 1967; Pfeifle et al., 1995). Systematic creep tests on Gorleben salt exhibit a factor of 1000 variation in strength of the rock salt in one salt succession (Hunsche et al., 2003). Different salt members of Zechstein formation pose different compositions, which might be very similar (90% halite or more) but result in difference in effective viscosity of each salt layer and alter the deformation pattern observed in our models. The deformation pattern of the different salt layers (z2, z3 and z4), which exist in Gorleben diapir, suggests that these layers perhaps have slightly different mechanical properties.

That the difference in mechanical properties of these layers affects the sinking direction of the anhydrite blocks is tested in models where salt layers are modeled with arbitrary chosen Newtonian rheology. Assuming that different salt layers have different effective viscosities (e.g., z2 layer is more viscose than the z3 and z4 layers) the anhydrite layer resting on stiffer salt descends relatively slower and without significant deformation (Fig. 10a). In this model, the lateral movement accompanies the fall of the anhydrite blocks, as the overlying salt layer is less viscous and deforms easier. Alternately, if the viscosity of the z2 layer is less than the viscosity of the z3 and z4 layers the anhydrite layer sinks easily within the less viscous salt (Fig. 10b). The anhydrite layer falls almost vertically and folds when it reaches the base. The deformed layer and blocks pile in less viscous salt (z2 layer).

It is evident that depending on size and orientation of the anhydrite layer deformation pattern is significantly different within the diapir (Fig. 11). Horizontal blocks sink much slower than vertical blocks. Furthermore, the rate of descent differs on different sides of the diapir. Descent rate, mode and pattern depend on vertical and horizontal location and orientation of the anhydrite blocks within the diapir. In

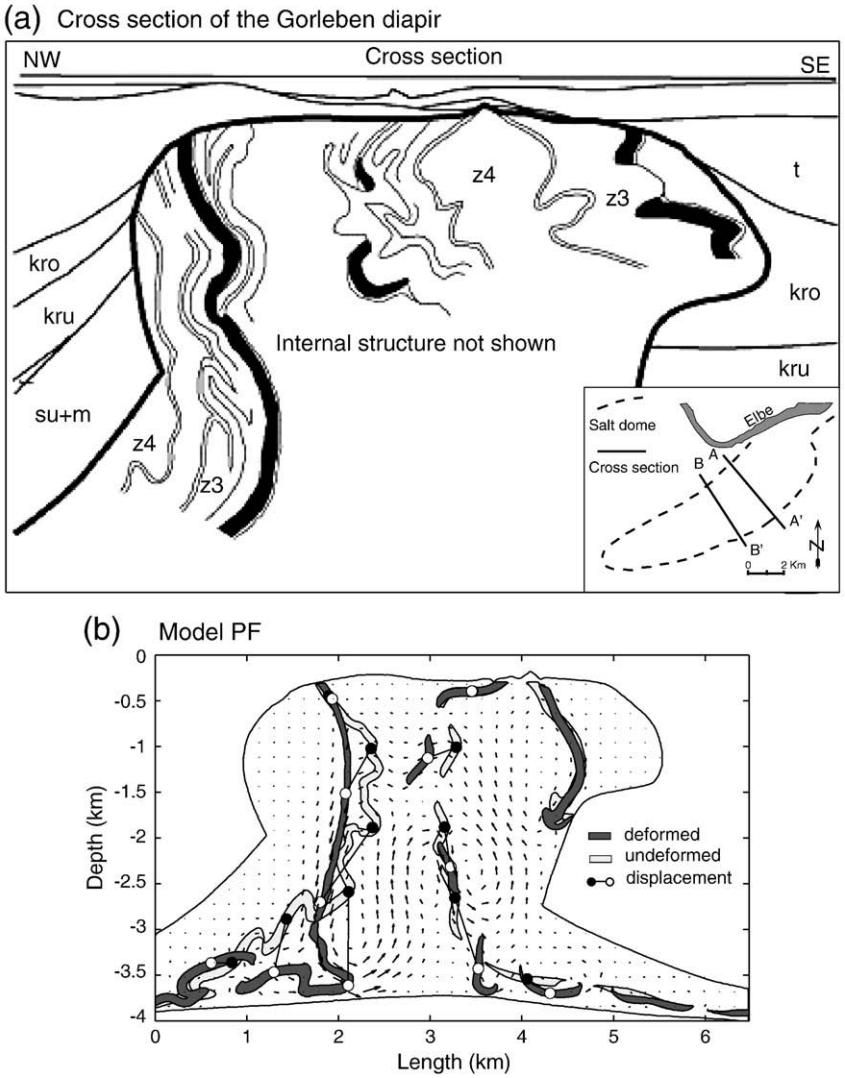

Fig. 11. Illustration of the anhydrite deformation within the Gorleben diapir and in model with Paradox Formation salt rheology. a) Northwest–southeast cross section (*BB′*) of the Gorleben diapir (cross section *AA′* is shown in Fig. 1). b) Internal deformation of the diapir (PF-Model) shown after 85 kyr. Arrows define velocity vectors at $t = 85$ kyr.

addition, in models with variable salt viscosity descent rate depends on the rheology of the salt, which is in direct contact with the anhydrite layer.

7. Conclusions

Numerical models show that salt structures with intercalated dense layers are internally active. We have shown that the mobility of anhydrite blocks depends on the effective viscosity of salt which has to be lower than a threshold value of around 10^{18}–10^{19} Pa s. During the post-depositional stage, the effective viscosity may fall below this threshold (e.g. due to changing temperature or migrating/diffusing water). The internal deformation of the salt diapir by the descending blocks increases with decrease in effective viscosity of salt. Unlike salt viscosities beyond the values 10^{20} Pa s, for the common range of the effective viscosity of salt (10^{17}–10^{20} Pa s) relatively high rate of descend is observed for the intercalated dense layers. The mobility of these dense layers directly influences any repository within the diapir. However, the rate of deformation that the repository undergoes is strongly dependent on salt rheology.

Acknowledgments

We thank Gabriele Marquart for comments on the manuscript. The Swedish Research Council (VR) provided funding. We further acknowledge the anonymous reviewers for constructive reviews.

References

Biot, M.A., 1965. Theory of viscous buckling and gravity instability of multilayers with large deformation. Bulletin of Geological Society of America 76 (3), 371–378.
Bornemann, O., 1982. Stratigraphy and tectonics of the Zechstein in Gorleben salt dome using drilling results. Zeitschrift der Deutschen Geologischen Gesellschaft 133 (2), 119–134.
Bornemann, O., 1991. Zur geologie des salzstocks Gorleben nach den Bohrergebnissen. Hannover, Germany, Bundesamt fur Strahlenschutz Schriften, Salzgitter 4 (91), 67.
Carter, N.L., Horseman, S.T., Russell, J.E., Handin, J., 1993. Rheology of rocksalt. Journal of Structural Geology 15 (9–10), 1257–1271.
Chemia, Z., Koyi, H., 2008. The control of salt supply on entrainment of an anhydrite layer within a salt diapir. Journal of Structural Geology 30 (9), 1192–1200.
Chemia, Z., Koyi, H., Schmeling, H., 2008. Numerical modelling of rise and fall of a dense layer in salt diapirs. Geophysical Journal International 172 (2), 798–816.
Fairhurst, C., 2002. Geomechanics issues related to long-term isolation of nuclear waste. Comptes Rendus Physique 3 (7–8), 961–974.
Hughes, M., Davison, I., 1993. Geometry and growth kinematics of salt pillows in the southern north sea. Tectonophysics 228, 239–254.
Hunsche, U., Hampel, A., 1999. Rock salt—the mechanical properties of the host rock material for a radioactive waste repository. Engineering Geology 52 (3–4), 271–291 (April).
Hunsche, U., Schulze, O., Walter, F., Plischke, I., 2003. Projekt gorleben. Thermomechanisches Verhalten von Salzgestein 9G2138110000. BGR, Hannover.
Jaritz, W., 1993. Die Geowissenschaftliche Untershchung des Salzstocks Gorleben auf seine Eingnung fr ein Endlager fr radioaktive Abfalle-Stand 1993. Geologisches Jahrbuch 142, 295–304.
Kirby, S., Kronenberg, A.K., 1987. Rheology of the lithosphere: selected topics. Reviews of Geophysics 25 (6), 1219–1244.
Koyi, H., 2000. Analogue modelling of entrainment of non-evaporitic rocks by salt diapirs. 8th World Salt Symposium, vol. 1–2, pp. 149–153.
Koyi, H., 2001. Modeling the influence of sinking anhydrite blocks on salt diapirs targeted for hazardous waste disposal. Geology 29 (5), 387–390.
Koyi, H.A., Mancktelow, N.S., 2001. Tectonic Modeling: A Volume in Honor of Hans Ramberg. Geological Society of America, Boulder.
Koyi, H., Schott, B., 2000. The rise and fall of denser blocks within salt diapirs. Bollettino di Geofisica Teorica ed Applicata 42 (1–2), 64–66.
Landolt-Boernstein, 1982. Numerical data and functional relationships in science and technology group, v: geophysics and space research. Physical Properties of Rocks, vol. 1a. Springer, New York, p. 373.
Muller, W.H., Schmid, S.M., Briegel, U., 1981. Deformation experiments on anhydrite rocks of different grain sizes: rheology and microfabric. Tectonophysics 78 (1–4), 527–543.
Onshore disposal committee, 1989. Research programme on geological disposal of radioactive waste in the Nederland's. Final report on phase 1, Part 1: description of the programme, results, conclusions.
Pfeifle, T.W., Vogt, T.J., Brekken, G.A., 1995. Correlation of chemical, mineralogic and physical characteristics of Gulf Coast dome salt to deformation and strength properties. RESPEC Inc., Rapid City. Contract No. 1–92.
Ramsay, J.G., 1967. Folding and Fracturing of Rocks. McGraw-Hill Book Company.
Rönnlund, P., 1989. Viscosity ratio estimates from natural Rayleigh–Taylor instabilities. Terra Nova 1, 344–348.
Schléder, Z., 2006. Deformation mechanisms of naturally deformed rocksalt. Ph.D. thesis, Von der Fakultät für Georessourcen und Materialtechnik der Rheinisch—Westfälischen Technischen Hochschule Aachen.
Schmeling, H., Babeyko, A., Enns, A., Faccenna, C., Funiciello, F., Gerya, T., Golabek, G.J., Grigull, S., Kaus, B., Morra, G., Schmalholz, S.M., van Hunen, J., 2008. A benchmark comparison of spontaneous subduction models—towards a free surface. Physics of the Earth and Planetary Interiors 171 (1–4) (December 2008), 198–223.
Spiers, C., Schutjens, P.M.T.M., Brzesowsky, R.H., Peach, C.J., Liezenberg, J.L., Zwart, H.J., 1990. Experimental determination of constitutive parameters governing creep of rocksalt by pressure solution. Deformation Mechanisms, Rheology and Tectonics. Geological Society, London; Special Publication, vol. 54, pp. 215–227.
Spies, T., Eisenblätter, J., 2001. Acoustic emission investigation of microcrack generation at geological boundaries. Engineering Geology 61 (2–3), 181–188.
Talbot, C.J., 1999. Ice ages and nuclear waste isolation. Engineering Geology 52 (3–4), 177–192 (Apr.).
Urai, J.L., Spiers, C.J., Zwart, H.J., Lister, G.S., 1986. Weakening of rock salt by water during long-term creep (nuclear waste disposal). Nature 324 (6097), 554–557.
Van Keken, P.E., Spiers, C.J., Van den Berg, A.P., Muyzert, E.J., 1993. The effective viscosity of rocksalt: implementation of steady-state creep laws in numerical models of salt diapirism. Tectonophysics 225 (4), 457–476.
Vendeville, B., Jackson, M., 1992. The rise of diapirs during thin-skinned extension. Marine and Petroleum Geology 9, 331–353.
Weijermars, R., Jackson, M.P.A., Vendeville, B., 1993. Rheological and tectonic modeling of salt provinces. Tectonophysics 217 (1–2), 143–174.
Weinberg, R.F., 1993. The upward transport of inclusions in Newtonian and power-law salt diapirs. Tectonophysics 228 (3–4), 141–150.
Weinberg, R.F., Schmeling, H., 1992. Polydiapirs: multiwavelength gravity structures. Journal of Structural Geology 14 (4), 425–436.
Zirngast, M., 1991. Die entwicklungsgeschichte des salzstocks gorleben-ergebnis einer strukturgeologischen bearbeitung. Geologisches Jahrbuch 132, 3–31.
Zirngast, M., 1996. The development of the Gorleben salt dome (northwest Germany) based on quantitative analysis of peripheral sinks. Salt Tectonics. Geological Society, Special Publication, London, vol. 100, pp. 203–226.